Available online at www.sciencedirect.com
ScienceDirect
Nanomedicine: Nanotechnology, Biology, and Medicine 3 (2007) 111–119
nanomedicine
www.nanomedjournal.com

Cellular Nanomedicine

Cell selective response to gold nanoparticles

Hirak K. Patra, MSc,[a] Shuvojit Banerjee, MSc,[b] Utpal Chaudhuri, MD,[c] Prabir Lahiri, PhD,[c] Anjan Kr. Dasgupta, PhD[a,*]

[a]*Department of Biochemistry, Calcutta University, Kolkata, India*
[b]*Guha Centre for Genetic Engineering and Biotechnology, Calcutta University, Kolkata, India*
[c]*Institute of Hematology & Transfusion Medicine, Medical College, Kolkata, India*

Received 27 December 2006; revised 3 March 2007

Abstract Gold nanoparticles (GNPs) are considered a potential probe to detect cancer. The present article investigates whether GNPs, even in the absence of any specific functionalization, induce any cell-specific response. We report GNP-induced death response in human carcinoma lung cell line A549. In contrast, the two other cell lines tested, BHK21 (baby hamster kidney) and HepG2 (human hepatocellular liver carcinoma), remained unaffected by GNP treatment. The specificity of the induction of the death response in A549 cells implies that GNPs do not universally target all cell types. Flow-cytometric studies indicated that the response was dose dependent and had a threshold effect (in A549). Gradual increase in GNP concentration induces a proportional cleavage of poly(ADP-ribose) polymerase. The programmed nature of the death response is implied, because such cleavage follows activation of caspases. Notably, at higher GNP concentration there was an asymmetric accumulation of GNPs in the periphery outside the cell nucleus of the A549 cells. This was confirmed by confocal microscopy, a green scattering (possibly, surface-enhanced Raman effect) appearing on selective z-slices of the image.

Key words: Gold nanoparticles; Death response; Cancer cell; Confocal microscopy; Flow cytometry

Potential benefits of nanomaterials in biomedical and industrial applications for human health and environment are now accepted in the literature [1,2]. In the biological context, recent reports focus on the effect of size, shape, bioavailability, uptake, and subcellular distribution of such nanomaterials. At the cellular level some important insights have come from studies on cellular response to carbon nanotubes [3,4], calcium selenide nanoparticles [5-7], and gold nanoparticles (GNPs) [8,9]. Because of its chemical inertness, gold has been used internally in humans for the past 50 years, from its use in teeth to implants to radioactive gold used in cancer treatment [10,11]. GNPs exhibit some special optical properties such as plasmon resonance, which is primarily a quantum phenomenon operative on the nanoscale. This means that GNPs make an interesting probe for studying some intricate biomolecular events including protein folding [12,13]. In addition, GNPs also serve as specialized microscopic probes to study cancer cells, because GNPs selectively accumulate in tumor cells, showing bright scattering [14,15]. The potential to use GNPs as a targeted drug delivery agent stems from the absence of any report on GNP-induced cytotoxicity [8]. Cytotoxicity is, however, a term whose biomedical implication depends on the context. It is essential to carefully distinguish between agents causing universal cytotoxic behavior and agents causing toxicity to specific cells. Many of the available inducers of cellular apoptosis (or necrosis) are often nonspecific to cell types or to receptors on the cell surface or in subcellular regions. Nano-inspired research in this direction has to directly or indirectly address this cell-specific or receptor-specific targeting problem at some stage.

No conflict of interest was reported by the authors of this paper.

* Corresponding author. Anjan Kr. Dasgupta, Calcutta University, 35 Ballygunge Circular Road, Kolkata, WB 700019 India.
E-mail address: adgcal@gmail.com (A.K. Dasgupta).

1549-9634/$ – see front matter © 2007 Elsevier Inc. All rights reserved.
doi:10.1016/j.nano.2007.03.005

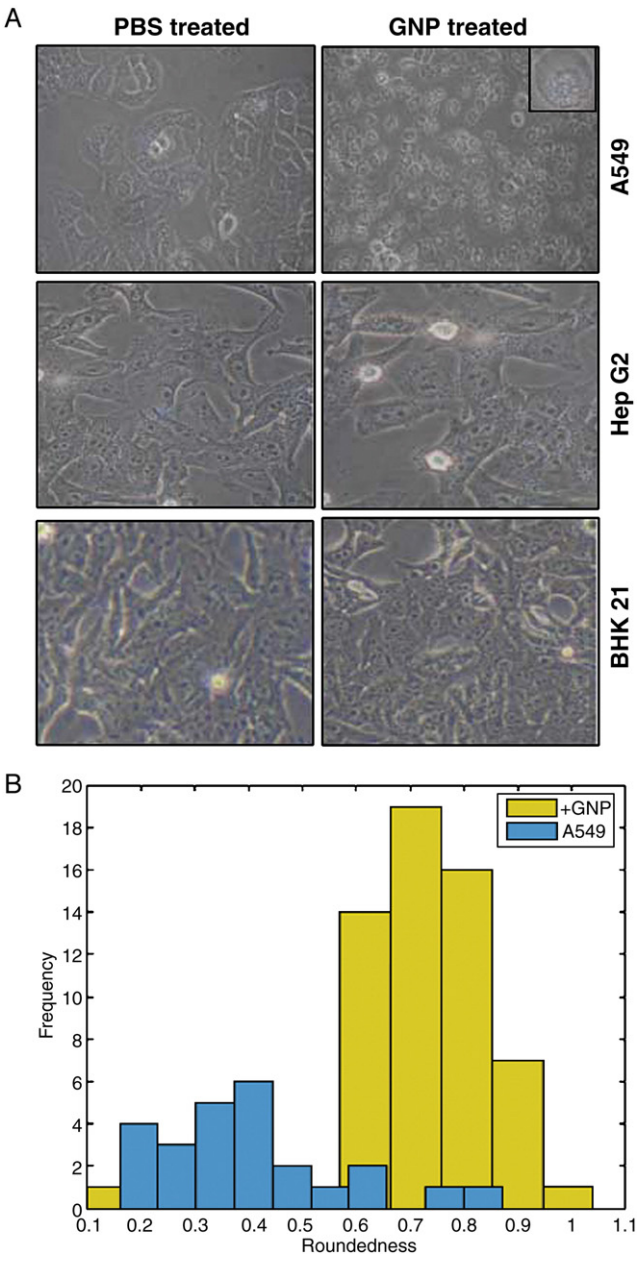

Fig 1. GNPs induced cellular morphology change in A549 cell line. **A,** Phase contrast images showing cellular morphologies of A549, BHK21, and HepG2 cell lines after treatment for 36 hours in the presence and absence (with PBS) of GNPs. Inset: magnified version of GNP-treated A549 cell. **B,** Quantitative representation by histogram of the cellular morphology change by roundedness of A549 cells after treatment with GNPs for 36 hours.

Incidentally, the cytotoxic effects of nanomaterials like quantum dots [16,17] or carbon nanotubes [18] extend even to normal, noncancer cells, and some debates have been raised on their unrestricted use. In contrast, with GNPs such issues do not arise and specific cell targeting is achieved using specific surface functionalization of the GNPs [15]. The underlying assumption is that GNPs themselves, being neutral, will not evoke any special cellular response, and the effect (if any) will be induced by the conjugated chemical group or biomolecule attached on its surface.

The issue of cell specificity in apoptosis or necrosis of cells mediated by nanoparticles, thus, may well be dictated by specific cell surface receptors and their characteristic distribution in those cells. The global cytotoxic effects, however, should be distinguished from this class of cell-specific (or cell receptor–specific) toxicity. In this article we consider responses induced by anion surface GNPs in different cell lines. Although we confirm that GNPs do not cause acute cytotoxicity [8] for certain cell lines, we have shown that in certain cancer cell lines the GNPs, even in the absence of any specific surface functionalization, have been able to induce apoptosis. The possible beneficial effect of this specific induction of the death response to certain types of cancer cells is indicated in the article.

Methods

GNP preparation

GNPs were prepared by the citrate reduction of $HAuCl_4$ following the methods of Storhoff et al [19]. Before the reduction process all glassware was cleaned in aqua regia (3 parts HCl, 1 part HNO_3), rinsed with nanopure H_2O, and then oven dried. An aqueous solution of $HAuCl_4$ (1 mM, 500 μL) was brought to boiling condition and stirred continuously with a glass rod. A 50-mL aliquot of a 38.8 mM trisodium citrate solution was added quickly at one time, resulting in a change in solution color from pale yellow to deep red. After the color change the solution was allowed to cool and was subjected to high-speed centrifugation. The pellet of GNPs was then resuspended in water at pH 7.0 after discarding the supernatant. The process was repeated three times to eliminate the free citrate.

Optical measurements

The plasmon band of the GNP solution was measured using an Analytik Jena (Jena, Germany) Spekol 1200 diode detector. The hydrodynamic size was measured using a Malvern Instruments NanoZS (Worcestershire, UK). The same instrument was used to measure the zeta potential of the GNP colloidal suspension. This technique efficiently measures the velocity of tiny particles within the fluid streams moving at the velocity of the fluid. The zeta potential is a purely electrokinetic property of the electrical double layer surrounding the subject but not the surface of the subject itself. Determining the electrophoretic mobility and then applying the value in Henry's equation measures this quantity. The velocity of a particle in an electric field is known as electrophoretic mobility (U_E). Now, applying this value to Henry's equation we obtain the value of the zeta potential.

Flow cytometry measurement

For this technique we have used FACSCalibur (BD Biosciences, San Jose, CA), which provides two excitation sources (488-nm air-cooled argon-ion laser and red diode laser He-Ne source with 635 nm). Population distributions

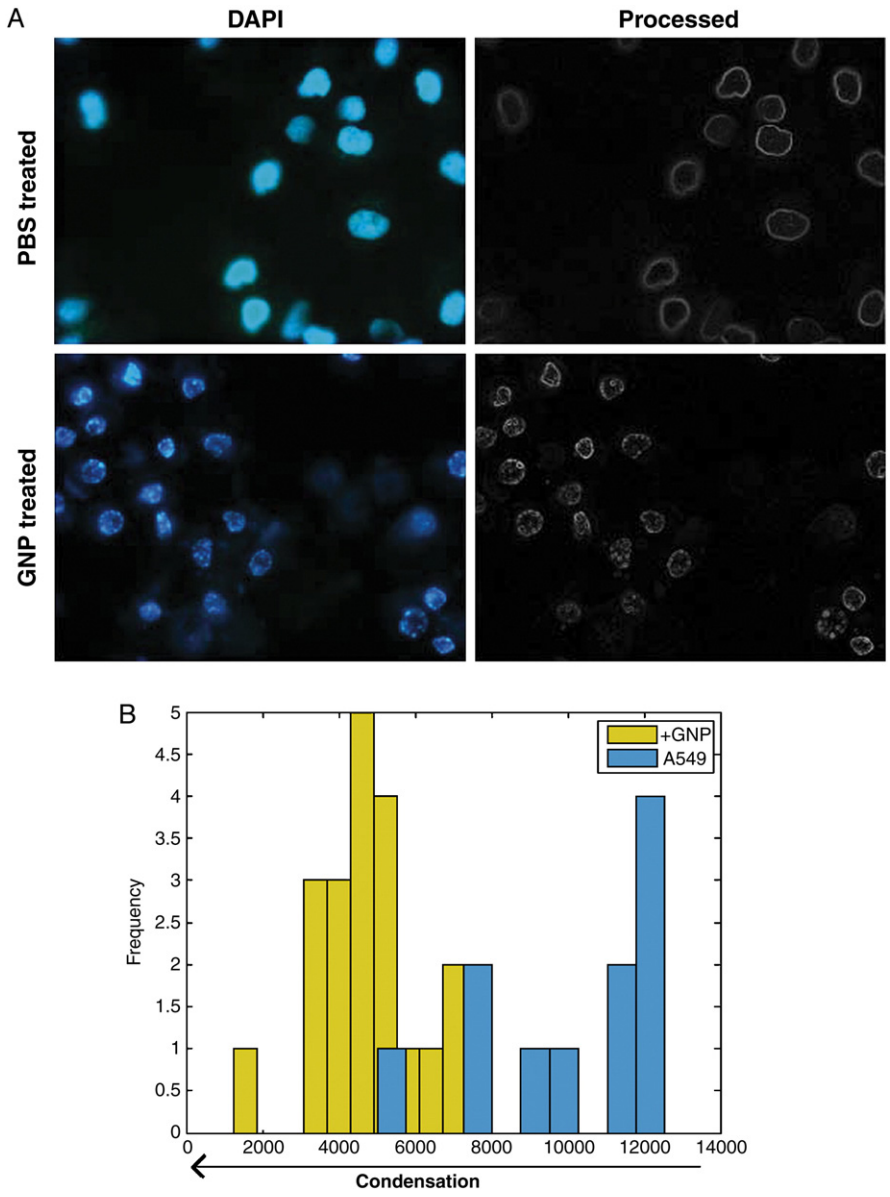

Fig 2. GNP induced nuclear morphology change in A549 cell line**. A,** Left column: fluorescence microscopic images of nuclear morphology in GNP-treated A549 cell after staining with DAPI along with control cells. Right column: processed images of nucleus to represent the nuclear condensation as well as nuclear fragmentation event in treated and untreated A549 cell line. **B,** Quantitative representation of the nuclear condensation event in treated and untreated A549 cells. The area (pixel units) is taken as the maximal DAPI-stained region per unit cell object.

of propidium iodide (PI)–labeled cells were detected by plotting the fluorescence Fl2 at 585 ± 21 nm against the forward scattering using the first excitation option. About 10,000 events/sample were acquired. The raw data obtained from flow cytometry are then subjected to analysis in Matlab 7.1 (Mathworks, Natick, MA) after suitable transfer of fluorescence-activated cell sorting (FACS) files.

Cell culture

Human Caucasian lung carcinoma type II epithelial cells, A549 cell line (obtained from National Centre for Cell Science, Pune, India) were routinely grown in Ham's F12 K medium with 10% heat-inactivated fetal bovine serum (both from GIBCO-BRL, Gaithersburg, MD) and 1% penicillin/streptomycin (GIBCO-BRL) at 37°C in a humidified 5% CO_2 atmosphere. Human Caucasian hepatocyte cells, HepG2 cell line, were provided by Dr. Samit Adhya (Indian Institute of Chemical Biology, Kolkata, India). HepG2 and Syrian hamster kidney fibroblast cells BHK21 were regularly grown in Dulbecco's modified Eagle medium supplemented with 10% heat-inactivated fetal bovine serum and 1% penicillin/streptomycin (all from GIBCO-BRL) at 37°C in a humidified 5% CO_2 atmosphere as described above. GNPs were used to induce cytotoxicity at the doses indicated. GNP stock was prepared at 2 mM in phosphate-buffered saline (PBS) (pH 7.2) for treatment. Treatments were carried out in 35-mm tissue culture plates (Axygen, Union City, CA). Following insult, cells were detached with

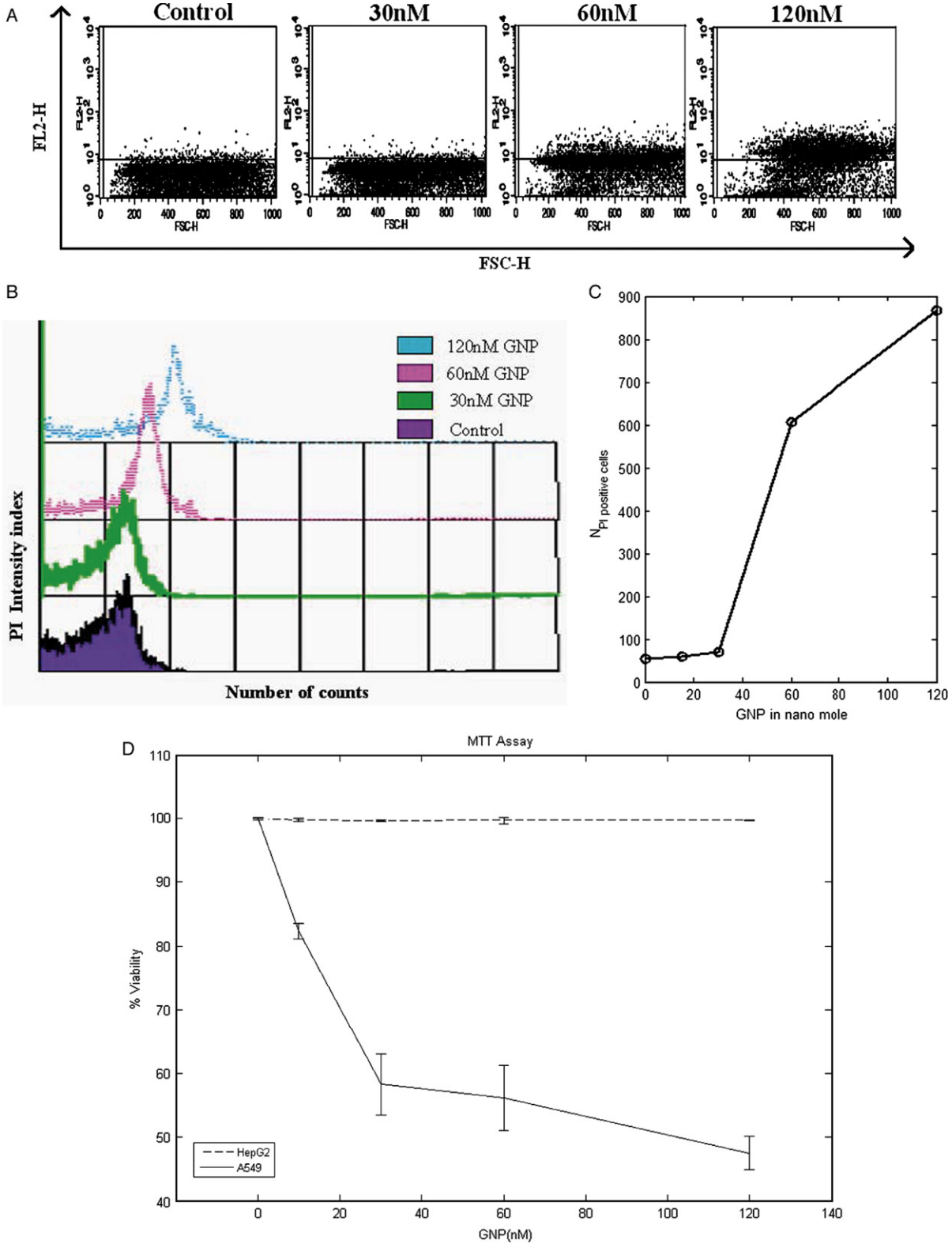

Fig 3. Flow-cytometric analysis of cytotoxicity by estimation of PI uptake in GNP-induced A549 cells. **A,** Dot plots show that treatment of A549 cells with GNPs leads to cell death in a concentration-dependent manner. **B,** The gradual shifting of the dead A549 cell population with increase in GNP concentration. **C,** The representative curve of A549 cell death (PI-positive cells) induced by different concentration of GNPs. **D,** MTT assay for viability of cells. Cell viability assay by MTT shows reduction in viability with variable concentrations of GNP-treated A549 cells represented by solid lines (—) but no significant effect observed in Hep G2 cells with the same treatment represented by the broken line (- - -).

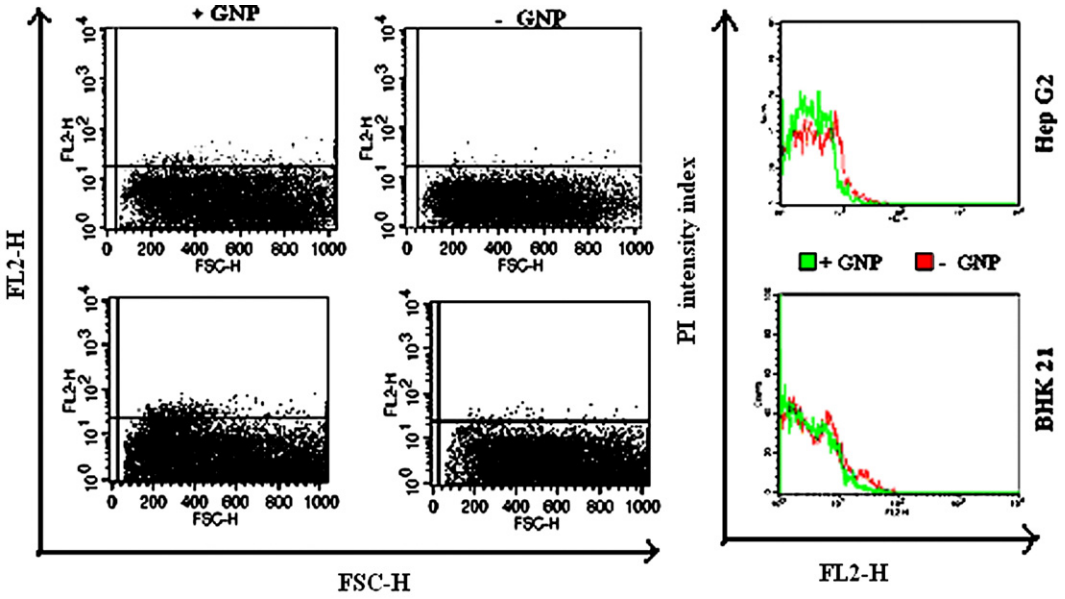

Fig 4. Flow-cytometric cytotoxicity assay by estimation of PI uptake in GNP-induced HepG2 and BHK21 cells. Dot plots along with PI intensity index show that there is no perceptible cell death induced by GNPs (120 nM) after incubation for 36 hours in HepG2 and BHK21 cell lines.

a trypsin-EDTA solution (Sigma-Aldrich, St. Louis, MO) and collected together with their supernatants for FACS analysis. Samples were collected after 36 hours for A549 and 72 hours for HepG2 and BHK 21, post-insult.

Analysis of cellular morphology change

All the control and treated cell lines were stained with excess PI to stain all the nucleic acids including RNA to visualize the complete cell at the desired wavelength compatible to the software used for image analysis. The cellular morphology images were obtained in an Olympus fluorescence microscope, equipped with Olympus Cool Snap Camera. The quantitative estimations were carried out by Micro-Image, Image tool (Olympus) and Matlab 7.1 from Mathworks. Cell morphology and z-slicing was also performed with Zeiss Confocal LSM510 Microscope (Oberkochen, Germany).

Analysis of nuclear morphology change

Nuclei of the treated and control cell lines were stained with DAPI and visualized using an Olympus fluorescence microscope equipped with an Olympus Cool Snap Camera (Tokyo, Japan). A minimum of 200 cells were counted and classified as follows: (1) live cells (normal nuclei: blue chromatin with organized structure); (2) stressed cells (bright-blue chromatin, which is highly condensed, marginated, or fragmented). The quantitative estimations were carried out by Micro-Image, Image tool, and Matlab 7.0 version softwares.

Cell cytotoxicity measurement

PI uptake measurement

PI (Sigma-Aldrich) was used to quantify cell death. Treated cells were collected as described above, washed once with ice-cold PBS (pH 7.2), and then resuspended to 1.0×10^5 cells/mL. PI was added before flow-cytometric analysis to a final concentration of 50 μg/mL.

MTT assay

Cell viability after treatment of chemicals is the routine method in toxicological assays. The MTT salt (3-(4,5-dimethylthiazol-2-yl)-2,5-diphenyl tetrazolium bromide) is reduced by mitochondrial dehydrogenases to the water-insoluble MTT formazan. The extracted MTT derivative was mixed with 1 mL of isopropyl alcohol with 0.04% HCl, and the absorbance values were determined at a 570-nm test wavelength and a 630-nm reference wavelength to test the cell viability. After treatment with various concentrations of GNPs the culture medium was replaced with serum-free medium containing 0.5 mg/mL MTT, and cultures were incubated for an additional 3 hours. The blue MTT formazan was dissolved in isopropyl alcohol with the specified percentage of HCl, and their absorbance values were measured using a Spekol 1200 (Analytik Jena) spectrophotometer. The untreated cells are used as a positive control (i.e., 100% viable), and all values from the experiment are correlated with this set of data. The results are displayed as percentage of viable cells compared with the control.

Cleavage of poly(ADP-ribose) polymerase

PARP is a 116-kDa nuclear poly(ADP-ribose) polymerase. This protein can be cleaved by many ICE-like caspases (named for their similarity to another kind of protease called the *i*nterleukin-1b *c*onverting *e*nzyme) in vitro. Cleavage of PARP serves as a marker of cells undergoing apoptosis.

Whole-cell extracts were prepared by lysing the GNP-treated cells suspended in lysis buffer (20 mM Tris pH 7.4, 250 mM NaCl, 2 mM EDTA pH 8.0, 0.1% Triton X-100,

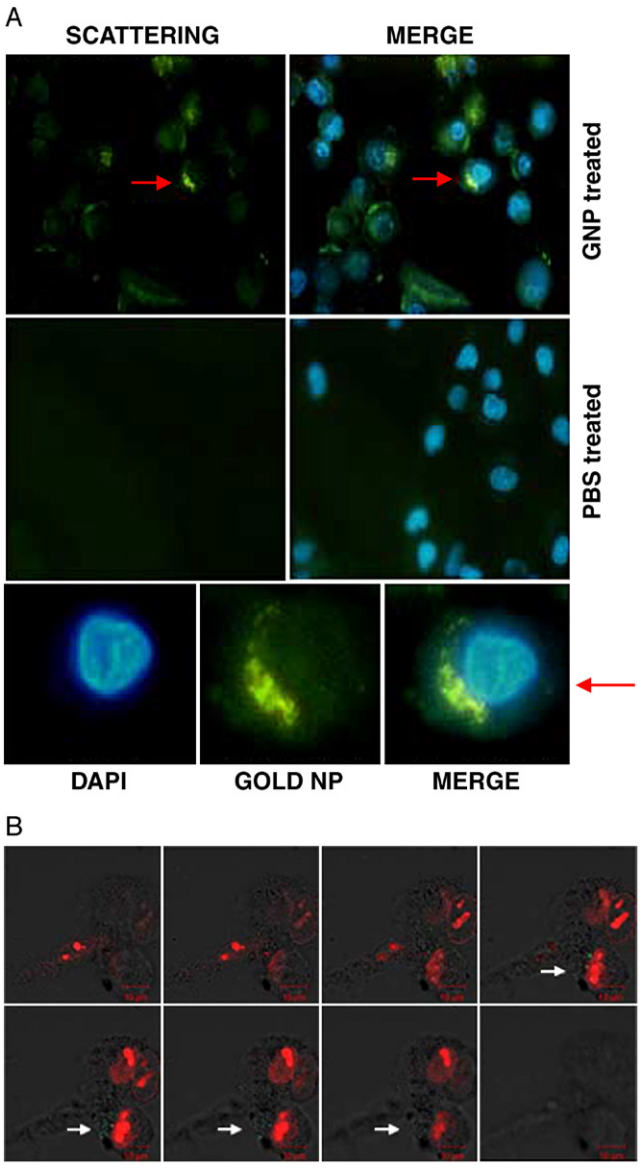

Fig 5. Intracellular localization of GNPs in A549 cells. **A,** Upper panel: The left column is the scattering of GNPs in the presence and absence of GNPs after excitation in the ultraviolet-visible range (300-450 nm). The right column shows the coexistence of nucleus (DAPI) and GNP scattering, in the presence and absence of GNPs. Lower panel: Magnified version of the red arrow marked cell. **B,** Confocal microscopic observation of GNP-treated A549 cell after staining with PI. Serial images (left to right) are the xy planes (z-slice) of the same cells at the continuative z-axis.

0.01 mg/mL aprotinin, 0.005 mg/mL leupeptin, 0.4 mM phenylmethanesulfonyl fluoride, and 4 mM $NaVO_4$). Lysates were then spun at 14,000 rpm for 10 minutes to remove insoluble material. The 30- to 50-μg cytoplasmic protein extracts were resolved by 8-12% sodium dodecyl sulfate–polyacrylamide gel electrophoresis. For tissue samples, the tissue was homogenized in lysis buffer. Protein concentration was measured using Bio-Rad protein estimation kit (BioRad, Richmond, CA). Thirty micrograms of tissue extract was resolved by sodium dodecyl sulfate–polyacrylamide gel electrophoresis. After electrophoresis, the proteins were electrotransferred to a PVDF membrane, blocked with 5% nonfat milk (Bio-Rad), and probed with antibodies (cell signaling) against PARP (1:1000) for 1 hour. Thereafter, the blot was washed, exposed to horseradish peroxidase–conjugated secondary antibodies for 1 hour, and finally detected by chemiluminescence (cell signaling). Whether the cytotoxic effect of a given inducer (GNPs in our case) is mediated through the apoptotic pathway can be evaluated from activation of PARP cleavage, because activated caspase-2, -3, and -7 are known to cleave PARP protein [20].

Results

Size distribution of GNPs using photon correlation spectroscopy

The plasmon resonance of the GNPs as measured using a diode detector (Analytik Jena) indicated a λ_{max} of the order of 524 nm. Photon correlation spectroscopy measurements (Malvern Instruments NanoZS) indicated the average hydrodynamic diameter (z average) of synthesized GNPs to be 33 nm with polydispersity of ~0.6. Doppler velocimetry revealed that the zeta potential of GNPs was around –22 mV (see Figures S1 and S2 in the Supplementary Material section of the online version of this article).

Cellular morphology change

A549 cells, grown in 35-mm sterile animal cell culture Petri dishes (Axygen), to approximately 70% confluency in a CO_2 incubator, then exposed to GNPs (0-120 nM) for 48 hours, showed changes in cellular morphology in response to GNPs. Phase contrast microscopy showed that the majority of the A549 cells became circular under the GNP-induced stress. Figure 1, *A* demonstrates the cellular morphology change in the A549 cell line along with the HepG2 cell line as cancerous cell control and BHK21 cell line as transformed cell control. The microscopic phase contrast images clearly show that the morphology changes in the other two cell lines (HepG2 and BHK21) are insignificant. The quantification of the morphology changes was studied using Image Tools software (University of Texas Health Science Center, San Antonio, TX, USA). The shape change was quantified with the extent of roundedness of the cell; one of the characteristics of stressed cells (Figure 1, *B*).

Nuclear morphology change

Again, exposure of nanomolar concentrations of GNPs without functionalization to human lung epithelial cancerous cells, A549, resulted in significant nuclear morphology changes, observed after staining with DAPI under a fluorescence microscope (Figure 2, *A*). The GNP-treated cells of the A549 line showed condensed nuclei. Nuclear condensation events due to stress are one of the most important signatures of cytotoxicity (see Figure S3 in the Supplementary Material section in the online version of this

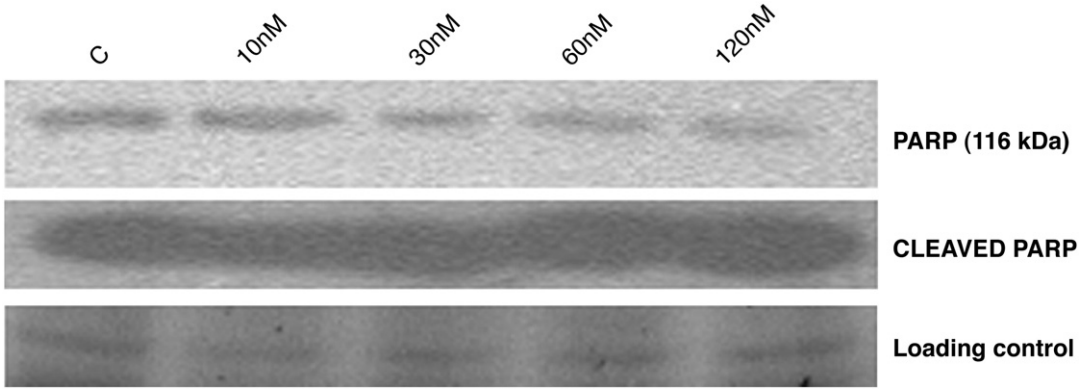

Fig 6. Western blot analysis for PARP. A549 cells were treated with different concentrations of GNPs for 48 hours. Activation PARP was analyzed by western blotting (detailed in Methods section). Treatment with GNPs activates PARP, as indicated by reduced levels of full-length PARP (upper panel) and increased levels of the active cleaved products (middle panel) with the increase of GNP concentration. The bottom panel represents the loading control.

article, which illustrates the nuclear fragmentation in GNP-treated A549 cells). The fluorescence microscopic images clearly show nuclear condensation in human lung epithelial cells of the A549 line, indicating an important selective effect of GNPs on cytotoxicity. The quantitative estimation of nuclear condensation by image processing further established the observation (Figure 2, *B*).

Flow-cytometric analysis of cytotoxicity

Cytotoxicity of GNPs was evaluated by measuring the cellular uptake of PI (Sigma-Aldrich) after treatment with GNPs for 48 hours in different nanomolar concentrations. Normally live cells are impermeable to PI, and PI uptake was used to quantify the population of cells in which membrane integrity was lost. Quantification of cell death was performed by FACS analysis [21]. Interestingly, GNP-treated A549 cells took up PI in a concentration-dependent manner. There was a gradual increase in the number of cells taking up PI with respect to increasing concentration of GNPs (Figure 3, *A*). There is a qualitative and relative change in the number of dead cells after GNP treatment (Figure 3, *B*). The gradual induction of cell death rises several fold beyond a 30 nM concentration of GNPs with increase in concentration. When we plotted the number of cells dead against GNP concentration (Figure 3, *C*) this induction showed a sigmoidal behavior. The PI uptake of GNP-treated HepG2 and BHK21 cell lines appeared to be almost identical to that with the untreated cells (Figure 4). So GNP-induced cytotoxicity is not universal to all cell lines.

Cell viability assay

Using the MTT assay the viability of A549 cells and control cells was measured at various concentrations (10-120 nM) of GNPs. Viability was measured in triplicate for two independent cell samples. Thus, at each different GNP concentration, effectively six viability measurements were available. In Figure 3, *D* the mean concentration is plotted against GNP concentration. The figure clearly illustrates that the A549 cells showed a rapid decrease of viability in the GNP concentration range 0-30 nM (see Figure 3, *D*), and this is followed by an attenuated decrease in the GNP concentration range 30-120 nM. In contrast, for HepG2 the viability remained unchanged over the said range of GNP concentration.

Confocal imaging of GNP-treated cells

The sensing, staining, and localization of GNPs were performed using fluorescence and confocal microscopic technique. The A549 cell line can be detected under a fluorescence microscope (Figure 5, *A*), in that it shows a green scattering. No such scattering was observed in other two cell lines. Moreover, the accumulation of GNPs was observed in a specific manner outside the nucleus in A549 cells. It is evident from the fluorescence microscopic (Figure 5, *A*) and confocal microscopic studies (Figure 5, *B*) that the GNP accumulation is localized in specific cellular domains (see the red-marked region in Figure 5, *A*, magnified in the lower panel). We can compare this observation with surface-functionalized nanoparticles tagged with a magneto-fluorescent nanoprobe that mimicked annexin and was used for sensing apoptotic cells, as reported in the study of Quinti et al [22] on fluorescent nanosensing of apoptotic cells. The confocal microscopic image (Figure 5*B*) shows the z-slicing of the GNP-containing A549 cell. The slicing reveals the existence of green scattering only in certain xy planes. It is also evident that the GNP accumulation occurs in the periphery of the nuclear region. The other remarkable feature is the asymmetric nature of the GNP distribution, the unipolar accumulation being also evident in the fluorescent microscopic images (see Figure 5, *A*).

Immunoblot analysis of PARP degradation

Figure 6 shows PARP distribution in control and GNP-treated cells. The five lanes indicate the distribution of PARP in the presence of GNP concentrations of 0, 10, 30, 60, and 120 nM, respectively. There is a clear indication

that with gradual increase in GNP concentration, the full-length PARP band becomes fainter and the cleaved band shows a compensatory increase in intensity. A loading control is used as reference in each case. The result implies that there is an inducer (GNP) concentration-dependent induction of caspases pathways that cleaves the PARP in a graded fashion.

Discussion

The primary observation that deserves mention is that the gold nanosurface, despite its chemical neutrality, evokes a cell-specific death response. Although the absence of such responses in certain cells (e.g., human leukemia [8]) is the case, it may not be universal for all cells or cell types. GNPs failed to induce any death response in cells like BHK21 or cancer cell lines like HepG2. The negative response in HepG2 cells is comparable to the earlier report on leukemia [8]. The induction of cell death in the human lung carcinoma cell line A549 has been shown to involve concentration dependence of the nanoform. Whereas loss-of-viability data and increase in PI uptake confirm that cytotoxicity is induced by GNPs, the cleavage of PARP implies that the cytotoxic effect is due to programmed cell death, because PARP cleavage is a terminal apoptotic node followed by both the intrinsic and extrinsic routes. The exact target of GNP within the cells is unclear at this stage. Notably, this is the first report describing apoptosis induction by GNPs. The external maneuverability of GNPs by photoactivation or induced hyperthermia opens the possibility of controlled and targeted induction of programmed cell death.

At high concentration GNPs accumulate at a region adjacent to the cell nucleus, the clustering being polarized in a small niche around the nucleus. This clustering was detectable in a fluorescent microscope and also by confocal imaging. The origin of this microscopically detectable inelastic scattering is also unclear. It could be a surface-enhanced Raman effect, a reported attribute of surface-clustered gold colloid [23,24].

Although these questions require more detailed future study, the point that we would like to highlight is that GNPs are more than a mere vehicle to carry specific antibodies to subcellular locations. There may be a direct crosstalk between GNPs and cellular and (or) subcellular receptors in certain cells. The understanding of the origin of such cell-specific responses may be an important step forward in nanomedicine involving gold.

Acknowledgments

The authors thank Prof. D.J. Chattopadhyay (Guha Centre for Genetic Engineering and Biotechnology, Calcutta University) for providing research material along with his help and suggestions. They also thank Prof. Samit Adhya (Indian Institute of Chemical Biology, Calcutta, India) for providing research materials and the Department of Science and Technology (India) for grant SR/SO/HS84/2004.

References

[1] Colvin VL. The potential environmental impact of engineered nanomaterials. Nat Biotechnol 2003;21:1166-70.
[2] Service RF. American Chemical Society meeting. Nanomaterials show signs of toxicity. Science 2003;300:243.
[3] Lam CW, James JT, McCluskey R, Hunter RL. Pulmonary toxicity of single-wall carbon nanotubes in mice 7 and 90 days after intratracheal instillation. Toxicol Sci. 2004;77:126-34.
[4] Kam NWS, Jessop TC, Wender PA, Dai HJ. Nanotube molecular transporters: internalization of carbon nanotube–protein conjugates into mammalian cells. J Am Chem Soc 2004;126:6850-1.
[5] Derfus AM, Chan WC, Bhatia S. Probing the cytotoxicity of semiconductor quantum dots. Nano Lett 2004;4:11-8.
[6] Daniel R, Larson WR, Zipfel RM, Williams SW, Clark MP, Bruchez FW, et al. Water-soluble quantum dots for multiphoton fluorescence imaging in vivo. Science 2003;300:1434-6.
[7] Wu X, Liu H, Liu J, Haley KN, Treadway JA, Larson JP, et al. Immunofluorescent labeling of cancer marker Her2 and other cellular targets with semiconductor quantum dots. Nat Biotechnol 2003;21:41-6.
[8] Connor EE, Mwamuka J, Gole A, Murphy CJ, Wyatt MD. Gold nanoparticles are taken up by human cells but do not cause acute cytotoxicity. Small 2005;1:325-7.
[9] Thomas M, Klibanov AM. Conjugation to gold nanoparticles enhances polyethylenimine's transfer of plasmid DNA into mammalian cells. Proc Natl Acad Sci U S A 2003;100:9138-43.
[10] Möhlen KH, Beller FK. Use of radioactive gold in the treatment of pleural effusions caused by metastatic cancer. J Cancer Res Clin Oncol 1979;94:81-5.
[11] Rosenberg SJ, Loening SA, Hawtrey CE, Narayana AS, Culp DA. Radical prostatectomy with adjuvant radioactive gold for prostatic cancer: a preliminary report. J Urol 1985;133:225-7.
[12] Chah S, Hammond MR, Zare RN. Gold nanoparticles as a colorimetric sensor for protein conformational changes. Chem Biol 2005;12:323-8.
[13] Bhattacharya J, Jasrapuria S, Sarkar T, GhoshMoulick RDasgupta AK. Gold nanoparticle based tool to study protein conformational variants: implications in hemoglobinopathy. Nanomedicine 2007;3:14-9.
[14] El-Sayed I, Huang X, El-Sayed MA. Surface plasmon resonance scattering and absorption of anti-EGFR antibody conjugated gold nanoparticles in cancer diagnostics; applications in oral cancer. Nano Lett 2005;4:829-34.
[15] El-Sayed I, Huang X, El-Sayed MA. Selective laser photo-thermal therapy of epithelial carcinoma using anti-EGFR antibody conjugated gold nanoparticles. Cancer Lett 2006;239:129.
[16] Bruchez MJ, Moronne M, Gin P, Weiss S, Alivisatos AP. Semiconductor nanocrystals as fluorescent biological labels. Science 1998;281:2013-6.
[17] Hardman R. A toxicologic review of quantum dots: toxicity depends on physicochemical and environmental factors. Environ Health Perspect 2006;114:165-71.
[18] Magrez A, Kasas S, Salicio V, Pasquier N, Seo JW, Celio M, et al. Cellular toxicity of carbon-based nanomaterials. Nano Lett 2006;6:1121-5.
[19] Storhoff JJ, Elghanian R, Mucic RC, Mirkin CA, Letsinger RL. One-pot colorimetric differentiation of polynucleotides with single base imperfections using gold nanoparticle probes. J Am Chem Soc 1998;120:1959-64.
[20] Oliver FJ, Rubia G, Rolli V, Ruiz-Ruiz MC, Murcia G, Murcia JM. Importance of poly (ADP-ribose) polymerase and its cleavage in apoptosis. Lesson from an uncleavable mutant. J Biol Chem 1998;273:33533-9.

[21] Nuria S, Violeta GV, Isabel M, Angel M, Thomas GC. Oxidative stress-induced apoptosis in retinal photoreceptor cells is mediated by calpins and caspases and blocked by the oxygen scavanger CR-6. J Biol Chem 2004;279:39268-78.

[22] Quinti L, Weissleder R, Tung C. A fluorescent nanosensor for apoptotic cells. Nano Lett 2006;6:488-90.

[23] YunWei CC, Rongchao J, Chad AM. Nanoparticles with Raman spectroscopic fingureprints for DNA and RNA detection. Science 2002;297:1536-40.

[24] Huang X, EI-Sayed IH, Wei Q, EI-Sayed MA. Cancer cell imaging and photothermal therapy in the near-infrared region by using gold nanorods. J Am Chem Soc 2006;128:2115-20.